



# UNIVERSITÀ DI PARMA

## ARCHIVIO DELLA RICERCA

University of Parma Research Repository

Advancement in measuring the hydraulic conductivity of porous asphalt pavements

This is the peer reviewed version of the following article:

*Original*

Advancement in measuring the hydraulic conductivity of porous asphalt pavements / Giuliani, F.; Petrolo, D.; Chiapponi, L.; Zanini, A.; Longo, S.. - In: CONSTRUCTION AND BUILDING MATERIALS. - ISSN 0950-0618. - 300:(2021), p. 124110.124110. [10.1016/j.conbuildmat.2021.124110]

*Availability:*

This version is available at: 11381/2895499 since: 2021-09-12T12:33:39Z

*Publisher:*

Elsevier Ltd

*Published*

DOI:10.1016/j.conbuildmat.2021.124110

*Terms of use:*

Anyone can freely access the full text of works made available as "Open Access". Works made available

*Publisher copyright*

note finali coverpage

(Article begins on next page)

# Advancement in measuring the hydraulic conductivity of porous asphalt pavements

F. Giuliani<sup>a</sup>, D. Petrolo<sup>a</sup>, L. Chiapponi<sup>1a</sup>, A. Zanini<sup>a</sup>, S. Longo<sup>a</sup>

<sup>a</sup>*Department of Engineering and Architecture, University of Parma, Parco Area delle Scienze 181/A, 43124 Parma, Italy*

---

## Abstract

The measurement of the in situ hydraulic conductivity of porous asphalt pavements,  $K$ , is a matter of practical interest; however, there are cases where current techniques are difficult to use. Several methods are documented in literature, mainly based on permeameters with water as fluid. Using water has its advantages, as it is straightforwardly related to the drainage problem during rain storms, but it also involves some major issues, especially on field studies. For instance, the time necessary to reach the steady state is too long and the necessary amount of water could not be available. In addition, non-repeatability and hysteresis phenomena can occur, also due to air bubbles confined in the porous matrix. In the present paper, we describe a novel test method for measuring  $K$  with the adoption of laboratory measurements for calibration with a glass beads porous medium using air at low pressure as fluid. The proposed permeameter was first tested in the laboratory, in order to (i) validate the theoretical relationships between  $K_{H_2O}$  and  $K_{air}$ , and (ii) define a model to evaluate an equivalent length scale for asphalt pavements,  $L_{eq}$ , as a function of the thickness of the porous layer (this is useful when one-dimensional formulations are adopted in the case of three-dimensional plates or in-situ measurements). Finally, the protocol and methodology were validated on two sites in Italy (Monza, Milan, and Poviglio, Reggio Emilia) where  $K_{air}$  was measured by the air field permeameter, and compared with  $K_{H_2O}$ , measured by a standard falling head permeameter. The technique allows the determination of the hydraulic conductivity on the basis of the ratio between pressure difference and flow rate, and of  $L_{eq}$ .

*Keywords:* Porous asphalt pavements, pollution management, hydraulic conductivity, permeameters

---

## 1. Introduction

Road safety during rainfall events is a major concern and has pushed the development of porous pavements able to drain most of the water and guarantee an adequate wet grip. The pervious materials, not only allow storm water to infiltrate and flow over an

---

<sup>1</sup>Corresponding author: luca.chiapponi@unipr.it  
*Preprint submitted to Construction and Building Materials*

5 impervious surface beneath, but also filter pollutants. In urban areas, these materials  
6 help managing run-off, reducing the peak discharge in the surface water bodies, as well  
7 as reducing noise [1, 2, 3, 4]. On the downside, a first disadvantage is represented by  
8 clogging effects happen: sediments and tyre rubber particles transported by runoff tend to  
9 deposit and block the interconnected pores, reducing the hydraulic conductivity [5, 6, 7].  
10 In addition, with the increase of clogging particles filling the voids in the wearing course of  
11 road pavements, the sound absorption by the pavement may be reduced up to a factor of  
12 25% [8]. A second relevant disadvantage is the formation of ice on motorways and roads  
13 in cold regions. To prevent this, salts or various organic compounds, which lower the  
14 freezing point of water, are spread, although with despite the non ecological consequences  
15 to the natural environment [9, 10, 11, 12]. To limit environmental pollution, fluids with  
16 programmed rheological behaviour, able to penetrate into the pores of draining road  
17 surfaces, can be used to reduce the hydraulic conductivity (and therefore the dispersion)  
18 of brines and/or organic mixtures used for anti-icing and de-icing. with environmental  
19 and economic advantages.

20 Since the hydraulic conductivity is a fundamental parameter for a proper functioning  
21 of porous asphalt pavements, and tends to be altered by the aforementioned phenomena,  
22 its value must be checked during construction and maintenance. In order to (i) check of  
23 the quality of porous asphalt pavements during construction, (ii) perform controls during  
24 maintenance, and (iii) check the effectiveness of the retardant fluids against brine loss  
25 due to highly permeable pavements, An accurate and low cost procedure for measuring  
26 the hydraulic conductivity is then required, with a simple and reliable use for in situ  
27 measurements.

28 Several methods have been proposed in literature to evaluate the hydraulic conduc-  
29 tivity of asphalt concrete and pavements, but only a few of them aim at measuring the  
30 hydraulic conductivity in situ. Water is the most frequently adopted fluid, because it  
31 is straightforwardly related to the drainage problem on roads and highways during rain  
32 storms.

33 Some standardised water permeameters are listed below.

34 The European Standard EN 12697-40:2005(E) [13] describes a method to determine  
35 the in situ relative hydraulic conductivity of porous pavements by means of a water  
36 permeameter. The methodology is low cost, easy to use and it ensures the repeatability  
37 of the measurements.

38 Other two largely used devices are the National Center for Asphalt Technology  
39 (NCAT) falling head permeameter and the constant head permeameters based on the  
40 American Society for Testing and Materials (ASTM) C1701/C1701M [14] and ASTM  
41 C1781/C1781M [15] methods. Even if both methods can effectively be used with all  
42 pavement types, the hydraulic conductivity values measured with the NCAT method  
43 can be 1 – 9 times higher than those measured with the ASTM method [16, 17].

44 A low cost falling head permeameter, the Laboratorio Caminos Santander (LCS)  
45 device, was also built by [6] according to the Spanish standard NLT 327/00 [18]. They  
46 modelled the hydraulic conductivity of their specimens with the Horton equations, with  
47 a satisfactory comparison with the in situ measurements.

48 Nevertheless, water is not the most convenient fluid to use when we are interested  
49 in measuring the hydraulic conductivity of porous asphalt pavements. The main reason  
50 is that the porous media of interest are generally not fully saturated and the analysis  
51 of the data requires a mathematical formulation with further complexities [see, e.g. [19].

52 In addition, the porous media should be saturated at the bottom, and tests should be  
53 performed in steady state conditions. This is not easily achievable in situ.

54 A more convenient way to evaluate the hydraulic conductivity is to use air as fluid  
55 instead of water. The main advantages are that (i) a little time is necessary to establish  
56 pressure flow equilibrium; (ii) tests can be repeated without the influence of residual  
57 water in the porous medium and without the disturbances due to air trapped in the  
58 meati; (iii) the nature of the test is non destructive, as the crack sizes are not affected by  
59 gas flows, if applied for short period and with a low average pressure, [20]. As a matter  
60 of fact, some physical phenomena induced by water may alter the hydraulic conductivity  
61 of pavements (e.g., the crack propagation and the effect of surface tension in unsaturated  
62 media). It is difficult to reproduce such effects at a laboratory scale or during field studies  
63 using water as a fluid, so air guarantee more reliable values of the conductivity of the  
64 undisturbed medium [21, 22].

65 A long list of experiments on conductivity measurements with the use of air is avail-  
66 able for a wide variety of porous media [23, 24, 25, 26, 27, 28, 22, 29]. Further details can  
67 be found in Varganega (2012) [30], where an extensive literature review on the conduc-  
68 tivity of asphalt concrete is presented. The author pointed out that field conductivity  
69 measurements do not match well with laboratory measurements, although there is some  
70 correlation. He took into consideration and described all the possible influencing fac-  
71 tors, as the air voids, the air voids connectivity, the mix gradation, the mixture binder  
72 content, the nominal maximum aggregate size and the lift thickness. Another possible  
73 explanation of the discrepancies is the possible anisotropy of the porous structure in as-  
74 phalt concrete. Both laboratory experiments [31] and computational simulations [32, 33]  
75 show that the conductivity in the horizontal direction is greater than the vertical.

76 Most of the literature methods are based on an integral approach and they do not  
77 go into diriment fluid mechanics details. For instance, we remind the readers that Darcy  
78 law is strictly valid in laminar regime, for Reynolds number  $Re \leq 10$ , and that it is  
79 replaced by other approximations for larger values of  $Re$ . In addition, non linear relation  
80 between gradient pressure and flow rate is often attributed to turbulence. As a matter  
81 of fact, turbulence is not triggered at the microscale of the voids of a porous medium.  
82 It is the sequence of contractions and expansions encountered by the fluid advancing in  
83 the porous matrix, or in the fissured medium, which induces Borda-Carnot losses.

84 A more detailed analysis is impeded by the evidence that many of the variables and  
85 parameters, such as path length and tortuosity, are known with limited accuracy. A rel-  
86 evant issue is the rheology of the fluid, which is Newtonian in most cases, but shows non-  
87 Newtonian behavior in some special cases. The slurry flowing on the asphalt pavement  
88 and infiltrating in the initial phase of heavy rainstorms after a long period of drought,  
89 with suspended particles and high concentration of pollutants, is prone to behave like an  
90 Ostwald-deWaele or Herschel-Bulkley fluid. This adds up further complexities, although  
91 several theoretical models of non-Newtonian fluids flowing in porous media [34, 35] and  
92 in fractures and fissures [36, 37] have been experimental validated. These aspects are  
93 left for future analysis with a perspective of improving the interpretation of hydraulic  
94 conductivity data for a better road and highway maintenance plan.

95 The main objective of this paper is to describe a very easy and immediate way to  
96 measure the in situ permeability of porous asphalt pavements, using air as fluid. We  
97 derive a very simple theoretical model based on the physics of the drainage process, to  
98 calculate an equivalent conductivity length scale,  $L_{eq}$ , as a function of the only thickness

of the porous asphalt layer. In situ, the only measurement of the ratio between pressure and inflow rate is required to evaluate the air conductivity of the asphalt pavements, together with the estimate of  $L_{eq}$ . Then, the water conductivity can be estimated on the basis of dimensional analysis.

First of all, to reach this goal, some cylindrical specimens made of glass beads were tested as a benchmark. The experimental value of the air conductivity,  $K_{air}$ , was compared with the water conductivity,  $K_{H_2O}$ , also obtained by empirical formulas found in literature. So, the conductivity ratio between the two fluids was found. In a second step, the air conductivity was measured both on asphalt plates and on cylindrical samples. Results were used to derive an equivalent length scale,  $L_{eq}$ , as a function of the thickness of the asphalt plate  $h$ . Finally, a series of field tests were conducted to compare the in situ air conductivity of a porous asphalt pavement with the water conductivity measured by a falling head permeameter. The experimental values of the ratio between conductivity to water and to air were also compared to the theoretical values predicted by dimensional analysis.

The paper is structured as follows. The theoretical approach to the problem is discussed in terms of dimensional analysis in § 2. The experimental setup and protocol are presented in § 3, while the results of laboratory tests and field cases are detailed in § 5. The conclusions are given in § 6.

## 2. Hints from dimensional analysis

Dimensional analysis can be used for a conceptual schematic of the fluid filtration processes in porous media and fractures and to retrieve similarity laws, see e.g. [38, 39] for details on the principles and applications. Filtration depends on geometrical variables related to the characteristics of the porous medium, like the diameter of the meat,  $D$ , the characteristic length path,  $L$ , and the porosity,  $n$ , and on the physical parameters of the fluid like the density,  $\rho$ , the dynamic viscosity  $\mu$ , and the velocity,  $u$ . Other physical quantities which influence the filtration processes are the acceleration due to gravity,  $g$ , and the total head,  $H$ , better considered as head variation  $\Delta H$ . In the presence of gas, also a slip between the gas molecules and solid walls occur, the so called Klinkenberg effect [40], with an increase of conductivity depending on the mean free path of molecules,  $l_m$ . In the most general case, we can describe the filtration process as a function of these variables and parameters:

$$f(\Delta H, L, \rho, g, D, u, \mu, n, l_m) = 0, \quad (1)$$

where  $n$  is already dimensionless. The rank of the dimensional matrix in a system of class  $M, L, T$  is three, hence relying on Buckingham's theorem we can express the process as a function of five dimensionless groups plus the porosity. Selecting a basis, e.g.  $D, \rho, g$ , a set of independent variables in a system of class  $M, L, T$ , the function of the possible dimensionless groups is

$$f' \left( \frac{\Delta H}{D}, \frac{L}{D}, \frac{u^2}{gD}, \frac{\rho Du}{\mu}, n, \frac{l_m}{D} \right) = 0, \quad (2)$$

where  $u^2/gD \equiv Fr$  is the Froude number,  $\rho Du/\mu \equiv Re$  is the Reynolds number,  $l_m/D \equiv Kn$  is the Knudsen number. Experimental evidences indicate that a more

138 suitable dimensionless group is the energy dissipation rate,  $J = -\Delta H/L$ , obtained as a  
 139 combination of  $\Delta H/D$  and  $L/D$ , and that  $L/D$  is not relevant if it is very large, in the  
 140 limit  $L/D \rightarrow \infty$ . Therefore, by expressing the  $J$  governed variable as a function of the  
 141 governing variables, we can write:

$$J = \tilde{f}(\text{Fr}, \text{Re}, n, \text{Kn}). \quad (3)$$

142 The Knudsen number for a gas can be computed adopting the expression of the mean  
 143 free path of molecules as a function of the temperature  $\theta$ , of pressure  $p$ , of the diameter  
 144 of the pores and of the Boltzmann's constant  $\kappa = 1.38 \cdot 10^{-23} \text{ J K}^{-1}$

$$l_m = \frac{\kappa}{\pi\sqrt{2}D^2} \frac{\theta}{p}, \quad (4)$$

145 hence

$$\text{Kn} = \frac{l_m}{D} \equiv \frac{\kappa}{\pi\sqrt{2}D^3} \frac{\theta}{p}. \quad (5)$$

146 Klinkenberg suggested that the gas intrinsic permeability varies as

$$k = k_\infty (1 + 8c \text{Kn}), \quad (6)$$

147 where  $k_\infty$  is the asymptotic intrinsic permeability for  $p \rightarrow \infty$  (or very large  $D$ ) and  $c$  is  
 148 an experimental coefficient slightly less than unity. A more common expression for the  
 149 intrinsic permeability for gases is

$$k = k_\infty \left( 1 + \frac{b}{p} \right), \quad (7)$$

150 where

$$b = 8c \frac{\kappa\theta}{\pi\sqrt{2}D^3} \quad (8)$$

151 is the Klinkenberg slip coefficient. In brief, increasing pressure/diameter reduces the  
 152 Knudsen number and the intrinsic permeability. It is noteworthy that Klinkenberg effect  
 153 is relevant only for low permeability media [41], found that the ratio between permeability  
 154 to argon and to water is of  $\mathcal{O}(10)$  for clay rich rocks], with typical values  $b = 10^3 - 10^5 \text{ Pa}$   
 155 for  $k = 10^{-12} - 10^{-18} \text{ m}^2$  [42], and is irrelevant for porous asphalt pavements with  
 156  $D = \mathcal{O}(10^{-3} \text{ m})$  even at an average ambient pressure, with  $\text{Kn} \rightarrow 0$ . As a general  
 157 consideration, we add that the formulation of Klinkenberg effect in terms of variation of  
 158 the intrinsic permeability (a geometric property) is odd: the effect of the slip is on the  
 159 flow, and should be better described in terms of variation of the conductivity.

160 On the basis of experimental evidence, eq.(3) is rearranged as:

$$\frac{\gamma JD}{\rho u^2} = \frac{\Phi(n)}{\text{Re}}, \quad (9)$$

161 where  $\Phi(n)$  is a function that depends on  $n$ . If we isolate  $u$ , we get:

$$u = \frac{1}{\Phi(n)} \frac{\gamma D^2}{\mu} J = KJ, \quad (10)$$

162 where  $K$  represents the conductivity. Equation (10) is the classical Darcy equation, valid  
 163 for small Re and also valid for gases if  $\text{Kn} \rightarrow 0$ .

164 The similarity condition requires the equality of Re and Fr and  $n$  in the two similar  
 165 processes, so we can write:

$$\begin{cases} \frac{r_\gamma r_J \lambda}{r_\rho r_u^2} = 1, \\ \frac{r_\rho r_u \lambda}{r_\mu} = 1, \\ r_n = 1. \end{cases} \quad (11)$$

166 where  $r_i$  is the scale ratio for the quantity  $i$ , and  $\lambda$  is the length scale. We are interested  
 167 in measuring the conductivity of a porous medium to air instead of water, for the case  
 168  $\lambda = 1$ . The scale ratios  $r_\rho$  and  $r_\mu$  are known parameters, so we can compute:

$$\begin{cases} r_J = r_u^2, \\ r_u = \frac{r_\mu}{r_\rho}. \end{cases} \quad (12)$$

169 The ratio  $r_\mu/r_\rho$  represents the scale ratio for the kinematic viscosity  $r_\nu$ , so  $r_\mu/r_\rho =$   
 170  $\nu_{\text{H}_2\text{O}}/\nu_{\text{air}} \approx 10^{-1}$ . Hence,

$$\begin{aligned} \frac{J_{\text{H}_2\text{O}}}{J_{\text{air}}} &\approx 10^{-2} \longrightarrow J_{\text{H}_2\text{O}} \approx 10^{-2} J_{\text{air}} \\ \frac{u_{\text{H}_2\text{O}}}{u_{\text{air}}} &\approx 10^{-1} \longrightarrow u_{\text{H}_2\text{O}} \approx 10^{-1} u_{\text{air}}. \end{aligned} \quad (13)$$

171 If the length path is the same, since we are dealing with the same porous medium  
 172 with the same geometry, we can also write

$$\Delta p_{\text{H}_2\text{O}} \approx 10^{-2} \frac{\gamma_{\text{H}_2\text{O}}}{\gamma_{\text{air}}} \Delta p_{\text{air}} \approx 10 \Delta p_{\text{air}}. \quad (14)$$

173 This means that at fixed Re and fixed Fr, the water pressure difference must be ten  
 174 times greater than the air, and the water velocity is ten times lower than air. Also  
 175  $Q_{\text{H}_2\text{O}} \approx 0.10 Q_{\text{air}}$ , since the cross-section area depends on  $\lambda = 1$ .

176 Finally, if we evaluate the scale ratio for the conductivity, using eq. (10), we obtain

$$r_K = \frac{K_{\text{H}_2\text{O}}}{K_{\text{air}}} = 10 \longrightarrow K_{\text{H}_2\text{O}} \approx 10 K_{\text{air}}. \quad (15)$$

### 177 3. Experimental set-up

178 The laboratory tests were carried out in the Laboratory of Hydraulics of the University  
 179 of Parma, the field tests were performed in Monza (Milan, Italy) and Poviglio (Reggio  
 180 Emilia, Italy). Three different permeameters were adopted, briefly described in the  
 181 following.

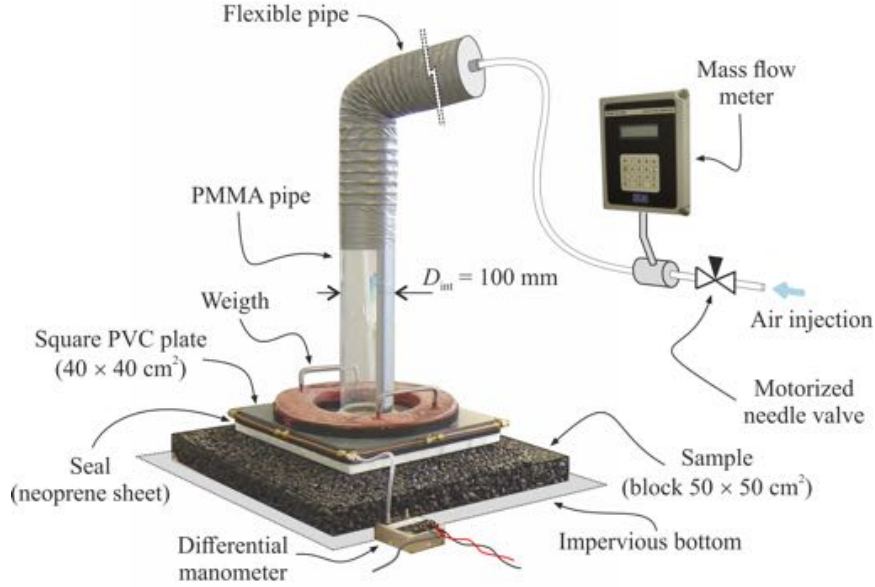


Figure 1: Experimental setup: the field permeameter.

### 182 3.1. Air field permeameter

183 Our experimental device is similar to the field permeameter used by [43], with a pipe  
 184 of Polymethylmethacrilate (PMMA) with internal diameter  $D_{\text{int}} = 100$  mm. The lower  
 185 end of the pipe is joined to a square plastic plate (polyvinyl chloride, PVC)  $40 \times 40$  cm<sup>2</sup>  
 186 and 2 cm thick, which must be placed on the asphalt plate, while the other end is  
 187 connected to the air supply line. A neoprene sheet is placed between the PVC and  
 188 the asphalt plates, and also vacuum grease is applied on the seal surfaces to avoid air  
 189 leakage. The pipe is long enough to allow the air jet exiting from a 8 mm tube to expand  
 190 and the flow to reach homogeneity before infiltrating in the porous medium. A circular  
 191 crown-shaped iron weight guarantees uniform and reproducible force on the square plate  
 192 in contact with the porous asphalt plate. The air flow rate is controlled by a motorized  
 193 needle valve, and is measured by a thermal mass flow meter (Kurz model 502-6A), with a  
 194 range  $0 - 1.00$  ls<sup>-1</sup> and with an accuracy of 2% FS. The differential pressure is measured  
 195 through a capacitive differential manometer (Ashcroft XLDP), with an accuracy of 0.5%  
 196 FS in a range  $0 - 65.0$  Pa. Before each test, the differential manometer was calibrated  
 197 with a calibrator Druck 601-F. The active port of the manometer is connected to the  
 198 PVC plate with several radial pipes, in order to average the pressure fluctuations, the  
 199 other port is connected to the atmospheric ambient. An electric valve also allows the  
 200 periodic connection of the active port to the atmospheric pressure, in order to correct  
 201 any bias. The experimental apparatus is shown in figure 1.

202 The instruments and the valves are controlled through a DAQ system with a data  
 203 rate of 20 Hz. All the tests are executed by progressively opening the needle valve and  
 204 acquiring the differential pressure and the air flow rate, and then progressively closing  
 205 the valve, up to the closure. This cycle is repeated twice.



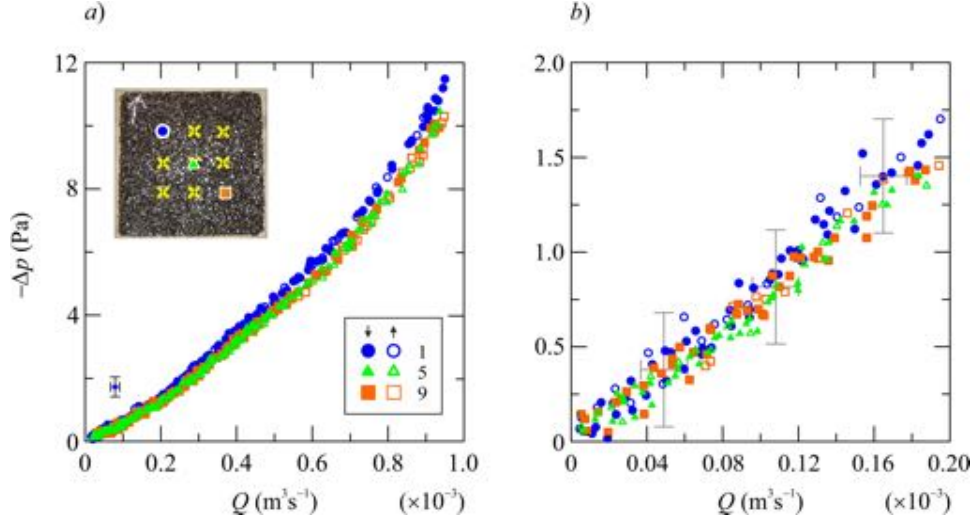


Figure 2: Pressure-discharge measurements for the 30 mm thick plate. *a*) Results for measurements with the permeameter centered in three different points shown in the inset; *b*) pressure-discharge measurements for the same experiment in *a*), in the limit  $Q < 0.20 \cdot 10^{-3} \text{ m}^3 \text{ s}^{-1}$ . Empty and filled symbols refer to the increasing and decreasing flow branch, respectively. Only one point in two hundreds is shown for clarity, with error bars equal to the instrumental accuracy.

206 Figure 2a shows the first cycle of increasing-decreasing air flow rate for the same  
 207 plate (thickness  $h = 30 \text{ mm}$ ) in three of the nine measurement points. Notice that it is  
 208 possible to center the permeameter in any position of the sample (ensuring a minimum  
 209 distance from the boundary), in order to estimate a possible non homogeneous behavior  
 210 of the asphalt plate. The selected measurement points are marked in figure 2a by dif-  
 211 ferent symbols and they are set 10 cm apart from one another, in both directions. The  
 212 measurement data show no hysteresis, with overlap of the branches of increasing and  
 213 decreasing air flow rate, and with a modest difference amongst the three sets of measure-  
 214 ments. The relationship flow rate–differential pressure is non-linear, as a consequence  
 215 of the Reynolds number which progressively increases beyond the limit of Darcy flow  
 216 regime. However, for  $Q < 0.20 \cdot 10^{-3} \text{ m}^3 \text{ s}^{-1}$  a linear trend is observed, as shown in  
 217 figure 2b, with a relationship:

$$-\Delta p = aQ, \quad (16)$$

218 where  $a$  is the slope of the interpolating straight line.

219 The Darcy law (10) can be written as:

$$K = \frac{u}{J} = -\frac{QL\gamma_{\text{air}}}{A\Delta p}, \quad (17)$$

220 where the velocity  $u$  is the ratio between the flow rate,  $Q$  and the cross-section area  $A$ ,  
 221 the average energy gradient,  $J = -\Delta H/L$ , is the change in the head  $\Delta H$ , over the length  
 222 path,  $L$ . If the fluid is air, one can write  $\Delta H = \Delta p/\gamma_{\text{air}}$ , with  $\gamma_{\text{air}}$  equal to  $12.02 \text{ N m}^{-3}$ .  
 223 Using eq. (16), eq. (17) becomes:

$$K = \frac{L\gamma_{\text{air}}}{8Aa}. \quad (18)$$

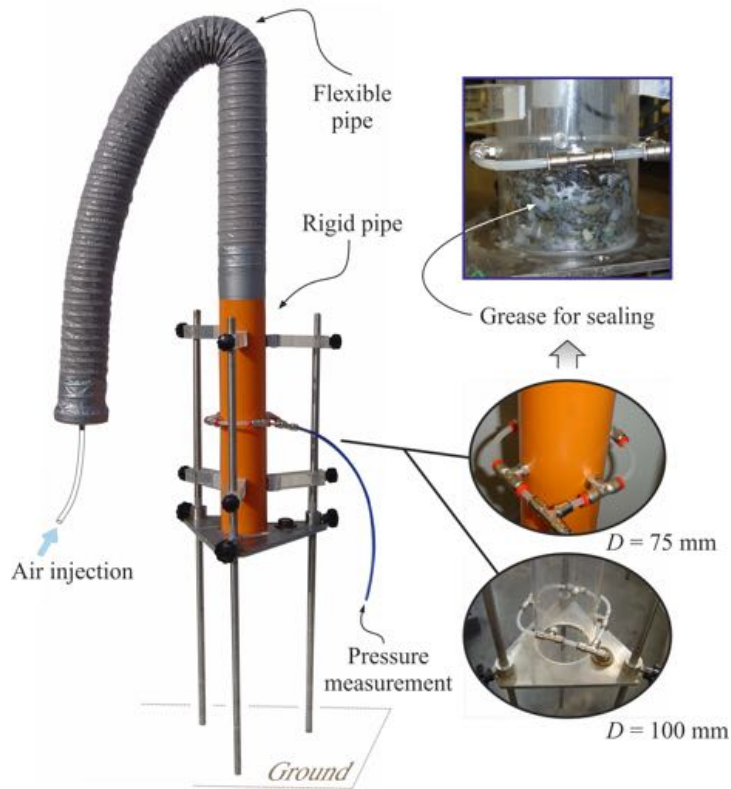


Figure 3: Experimental setup: 1-D permeameter.

224 *3.2. 1-D air laboratory permeameter*

225 In addition to the permeameter described in § 3.1, the permeameter shown in figure 3  
 226 has been constructed in order to estimate the one-dimensional (1-D) conductivity of the  
 227 asphalt sample.

228 The 1-D permeameter consists of a rigid pipe with diameter equal to 75 mm or  
 229 100 mm (two versions with different diameter,  $D$  were realized). The lower end of the  
 230 pipe is designed to laterally confine a cylindrical sample extracted from the asphalt plates,  
 231 and the sealing between the sample and the inner surface of the pipe is secured by the  
 232 application of vacuum grease. The other end of the pipe is connected to the air supply  
 233 circuit. The experimental procedure and all the instruments are the same as described  
 234 for the field permeameter in § 3.1, with the only difference that the active port of the  
 235 manometer is directly connected to the pipe by means of four radial intakes located in a  
 236 section a few centimetres above the sample.

237 *3.3. Water falling head permeameter*

238 A third permeameter was used to measure the hydraulic conductivity in situ. The  
 239 falling head permeameter used for this purpose is shown in figure 4. This permeameter

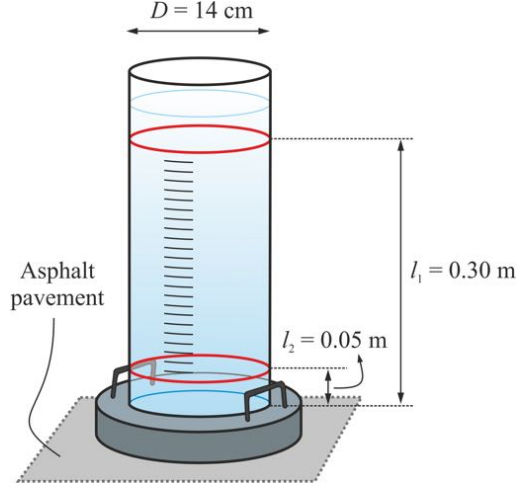


Figure 4: Falling head permeameter.

240 has a diameter of 14 cm and a total height of 35 cm. The hydraulic conductivity can be  
 241 computed as

$$K_{\text{H}_2\text{O}} = \frac{Ah}{A' \Delta t} \ln \left( \frac{l_1}{l_2} \right) \quad (19)$$

242 where  $A$  is the cross-section area of the standpipe,  $h$  is the thickness of the asphalt plate,  
 243  $A'$  is the sample cross-section, here equal to  $A' = A$ , and  $\Delta t$  is the recorded time interval  
 244 for the water column to flow through the sample, from the initial level  $l_1 = 0.30$  m to the  
 245 final level  $l_2 = 0.05$  m.

## 246 4. Materials and methods

### 247 4.1. Glass beads specimens

248 Some specimens with different mixtures of glass beads with diameter  $d = 1, 2, 3$  mm  
 249 were tested with the 1-D permeameter with air, for an estimate of the scale factor  $r_K =$   
 250  $K_{\text{H}_2\text{O}}/K_{\text{air}}$ . We prepared (i) homogeneous specimens, using uniformly sized beads; (ii)  
 251 stratified specimens, with three homogeneous horizontal layers of beads with increasing  
 252 diameter from top to bottom (1 – 2 – 3 mm) and vice-versa (3 – 2 – 1 mm); (iii)  
 253 heterogeneous mixtures by randomly mixing the beads of 1, 2, 3 mm, or 2, 3 mm, or  
 254 1, 3 mm. All the specimens have a diameter of 90 mm and height of 60 mm. The  
 255 porosity of approximately  $n \approx 37\%$  and the void ratio  $e = n/(1 - n) \approx 60\%$  were  
 256 measured as described by [44]. The specimens were placed inside a special holder with  
 257 a grid at the base that could hold the beads and support the weight of the specimen,  
 258 without interfering with the air flow. An O-ring seal was inserted between the holder  
 259 and the inner radius of the permeameter in order to prevent any air leakage.

260 A limited number of specimens (tests 3–4–5–9–10 of table 1) were also tested with  
 261 a standard 1-D permeameter (Matest S245-01) with water. This device is commonly used  
 262 to determine the permeability of granular, gravel and sand soils. The specimen is formed

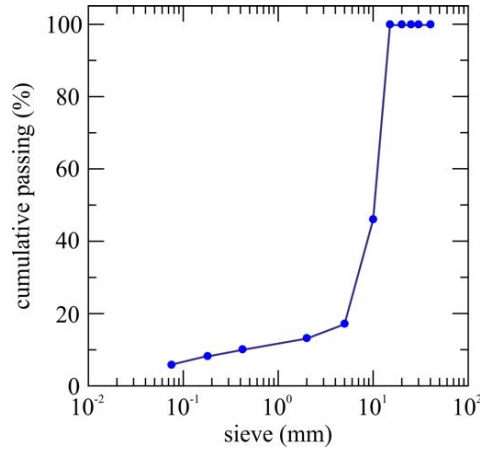


Figure 5: Aggregate grading curve of the porous asphalt square plates.

263 in an acrylic permeability cell, and water is passed through it from a constant level tank.  
 264 The permeability cell has pressure points at different levels which are connected to the  
 265 manometer tubes fixed on a stand with graduated scale.

#### 266 4.2. Porous asphalt square plates and cylindrical samples

267 In order to reproduce common draining asphalt plates, we built porous asphalt square  
 268 plates,  $50 \times 50 \text{ cm}^2$ , with variable thickness, with a discontinuous aggregate grading  
 269 curve, a polymer modified asphalt content of 4.2% by weight of aggregate, and a void  
 270 ratio of 17%. The aggregate grading curve is shown in figure 5. The polymer modified  
 271 asphalt was produced by ENI Company and has the following characteristics: PMA  
 272 50/70-93.5, penetration at  $25^\circ\text{C} = 5.5 \text{ mm}$  according to UNI EN 1426:2015 (included  
 273 into “Specifications for paving grade bitumens” EN 12591:2009). The binder performance  
 274 grade is PG 82-22 according to AASHTO M-320 Edition 2017. The glass fiber content  
 275 is 0.3% by weight of the aggregate.

276 The density of the samples was approximately  $2000 \text{ kg m}^{-3}$ . The samples were pre-  
 277 pared by (i) heating up the mixture in a furnace at  $180^\circ\text{C}$  for 6-8 hours; (ii) spreading  
 278 the mixture in a metallic framework; (iii) pressing it with a mechanical press which sim-  
 279 ulates the action of road rollers and homogenizes the thickness of the plate; (iv) further  
 280 compacting the mixture with a mechanical arm handling a cylindrical sector that repro-  
 281 duces the field compaction, as shown in figure 6a. The thickness of the plates were set at  
 282  $h = 30, 45, 65, 70$  and  $105 \text{ mm}$ . As in real road pavements, where an impervious interface,  
 283 made of a hot bituminous emulsion, is usually present beneath the porous near surface  
 284 layers, we positioned the asphalt plates on an impervious surface, but made of wood. A  
 285 typical example of asphalt plate is shown in figure 6c.

286 After the square plates were tested with the field permeameter, they were cored  
 287 for measuring the vertical 1-D conductivity by means of a core drill, as illustrated in  
 288 figure 6b.

289 In order to guarantee a sufficient lateral confinement, we decided to extract cylin-  
 290 drical samples with a diameter of  $75 \text{ mm}$  vertically from the central area of each plate.

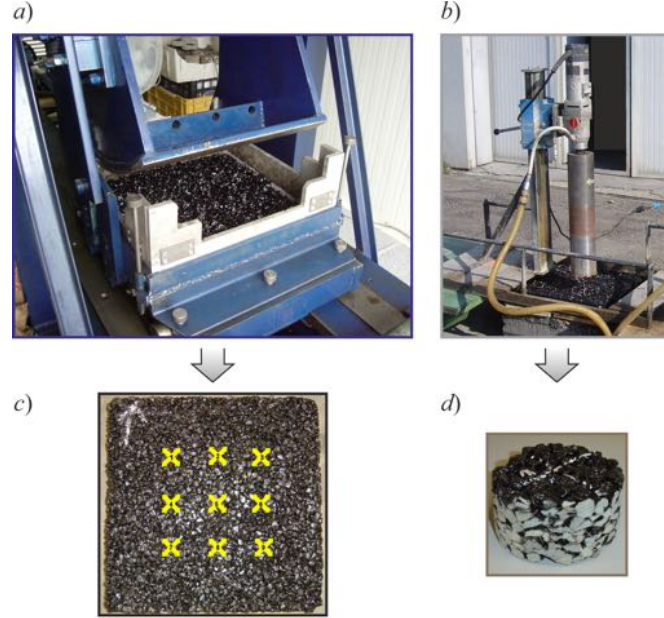


Figure 6: Preparation of the plates and samples. *a)* Laboratory machine used to create asphalt plates with variable thickness and  $50 \times 50 \text{ cm}^2$ ; *b)* driller coring the asphalt plates; *c)* asphalt plate ready to be tested with nine markers for the  $K_{\text{air}}$  measurements and an arrow indicating the top surface of the plate; *d)* sample cored from the plate, to be tested with 1-D permeameter.

291 Unfortunately, all the samples cored from the 30 mm thick plate crumbled, while only  
 292 one sample from the 45 mm thick plate survived. From the 65 mm thick plate we cored  
 293 three samples with a diameter of 75 mm and five samples with a diameter of 100 mm  
 294 in order to compare different geometries. From the 105 mm thick plate we extracted  
 295 two cores, with height of 65 mm. A typical example of cylindrical sample is shown in  
 296 figure 6d. We also attempted to core samples in the horizontal direction in order to  
 297 study possible anisotropy effects, but due to the limited thickness of the plates it was  
 298 not possible to guarantee the necessary lateral confinement.

#### 299 4.3. Experimental plan

300 Table 1 lists all the experiments in the laboratory.

301 Two further series of field tests were run in two available field sites. For some of  
 302 the field tests, the results for the air conductivity,  $K_{\text{air}}$ , were compared with the water  
 303 conductivity,  $K_{\text{H}_2\text{O}}$  measured by the falling head permeameter. The data collected on a  
 304 service road inside the Monza (Milan, Italy) racetrack are listed in table 2, where  $\Delta t_1$ ,  
 305  $\Delta t_2$ ,  $\Delta t_3$  are three measurements with the falling head permeameter and  $\bar{\Delta t}$  is the mean  
 306 value. The data collected on a urban road under construction in Poviglio (Reggio Emilia,  
 307 Italy) are listed in table 3.

test #	Permeameter	Medium	$d$ (mm)	$h$ (mm)	$D$ (mm)	$a$ (Pa m <sup>-3</sup> s) ( $\times 10^5$ )	$K_{\text{air}}$ (m s <sup>-1</sup> ) ( $\times 10^{-3}$ )	$K_{\text{H}_2\text{O}}$ (m s <sup>-1</sup> ) ( $\times 10^{-3}$ )
1	1D	GBh	0.5	60	90	3.422	0.40	
2	1D	GBh	0.75	60	90	3.074	0.44	
3	1D	GBh	1	60	90	1.805	0.64	10.59
4	1D	GBh	2	60	90	0.599	1.85	30.68
5	1D	GBh	3	60	90	0.316	3.87	56.3
6	1D	GBs	1-2-3	60	90	0.929	1.22	
7	1D	GBs	3-2-1	60	90	0.974	1.16	
8	1D	GBm	1,2,3	60	90	1.123	1.01	
9	1D	GBm	1,3	60	90	1.584	0.72	11.24
10	1D	GBm	2,3	60	90	0.439	2.58	31.91
11	1D	A	-	45	75	0.151	8.11	
12	1D	A	-	65	75	0.282	6.27	
13	1D	A	-	65	100	0.130	7.68	
14	1D	A	-	65	75	0.301	5.88	
15	F	A	-	30	100	0.064	6.79	
16	F	A	-	45	100	0.044	7.56	
17	F	A	-	65	100	0.048	5.69	
18	F	A	-	70	100	0.038	6.92	
19	F	A	-	105	100	0.030	7.44	

Table 1: List and parameters of the laboratory experiments. “F” stands for field permeameter (used in the laboratory with square asphalt plates) and “1D” for the 1-D permeameter. The medium is indicated by the following abbreviations: “A” stands for asphalt plate and “GB” for glass beads. In the case of experiments performed with glass beads of different size, GBh stands for homogeneous specimens, GBs for stratified specimens while GBm for an heterogeneous mixtures.  $d$  is the diameter of the glass beads,  $h$  is the thickness of the plate,  $D$  is the internal diameter of the permeameter,  $a$  is the inclination of the straight line fitting the  $(-\Delta p, Q)$  data,  $K_{\text{air}}$  is the air conductivity and  $K_{\text{H}_2\text{O}}$  is the water conductivity.

test #	$a$ (Pa m <sup>-3</sup> s) ( $\times 10^5$ )	$K_{\text{air}}$ (m s <sup>-1</sup> ) ( $\times 10^{-3}$ )	$\Delta t_1$ (s)	$\Delta t_2$ (s)	$\Delta t_3$ (s)	$\overline{\Delta t}$ (s)	$K_{\text{H}_2\text{O}}$ (m s <sup>-1</sup> ) ( $\times 10^{-3}$ )
M1	0.909	0.28	41	47	-	44	2.9
M2	0.735	0.35	-	-	-	-	-
M3	0.881	0.29	-	-	-	-	-
M4	0.686	0.38	34	38	-	36	3.5
M5	0.647	0.40	-	-	-	-	-
M6	0.599	0.43	-	-	-	-	-
M7	0.589	0.44	-	-	-	-	-
M8	0.545	0.47	28	31	33	31	4.1
M9	0.476	0.54	-	-	-	-	-
M10	0.444	0.58	-	-	-	-	-
M11	0.449	0.57	-	-	-	-	-
M12	0.570	0.45	22	23	-	23	5.6
M13	0.617	0.42	-	-	-	-	-
M14	0.621	0.41	-	-	-	-	-
M15	0.633	0.41	27	28	29	28	4.5
M16	0.605	0.43	-	-	-	-	-
M17	0.566	0.46	-	-	-	-	-

Table 2: List of the field tests performed in Monza on a porous asphalt pavement with thickness  $h = 70$  mm.  $K_{\text{air}}$  was estimated with the field permeameter,  $K_{\text{H}_2\text{O}}$  with the falling head permeameter.

test #	$a$ (Pa m <sup>-3</sup> s) ( $\times 10^5$ )	$K_{\text{air}}$ (m s <sup>-1</sup> ) ( $\times 10^{-3}$ )	$\Delta t$ (s)	$K_{\text{H}_2\text{O}}$ (m s <sup>-1</sup> ) ( $\times 10^{-3}$ )
P1	0.350	1.01	-	-
P2	0.247	1.43	16.65	4.3
P3	0.307	1.15	-	-
P4	0.446	0.79	-	-
P5	0.301	1.17	12.15	5.9
P6	0.524	0.67	-	-
P7	0.448	0.79	-	-
P8	0.404	0.88	14.25	5.0
P9	0.441	0.80	-	-
P10	0.283	1.25	-	-

Table 3: List of the field tests performed in Poviglio on a porous asphalt pavement with thickness  $h = 40$  mm.  $K_{\text{air}}$  was estimated with the field permeameter,  $K_{\text{H}_2\text{O}}$  with the falling head permeameter.

308 **5. Results**

309 *5.1. Validation of the theoretical model*

310 To prove that the conductivity scale ratio  $r_K = \mathcal{O}(10)$ , as predicted by dimensional  
 311 analysis in §2, we performed tests 1–7 listed in table 4. The experimental values of the air  
 312 conductivity,  $K_{\text{air}}$ , were computed according to eq. (18), considering a length path equal  
 313 to the height of the sample,  $h = 65$  mm, the cross-section area  $A$  of the permeameter,  
 314 and the parameter  $a$ .

315 On the other side, the value of the hydraulic conductivity for water,  $K_{\text{H}_2\text{O}}$ , was  
 316 calculated following different approaches [45].

317 Terzaghi (1925) [46] proposed that the hydraulic conductivity should be computed as  
 318

$$K_{\text{H}_2\text{O}} = \frac{g}{\nu} C_T \left( \frac{n - 0.13}{\sqrt[3]{1 - n}} \right)^2 d_{10}^2, \quad (20)$$

319 where  $C_T = 10.7 \cdot 10^{-3}$  for smooth grains, while according to [47]:

$$K_{\text{H}_2\text{O}} = \frac{g}{\nu} C_Z \left( \frac{n}{1 - n} \right)^2 d_e^2, \quad (21)$$

320 where  $C_Z = 2.4 \cdot 10^{-3}$  for uniform sand with smooth and rounded grains. Sauerbrey  
 321 (1932) [48] proposed that:

$$K_{\text{H}_2\text{O}} = \frac{g}{\nu} C_S \frac{n^3}{(1 - n)^2} d_{17}^2 \quad (22)$$

322 for soils with an effective diameter up to 5 mm, with  $C_S = 3.75 \cdot 10^{-3}$ . The equation  
 323 derived by Kozeny-Carman [49] can be used for silts, gravel and gravel sands:

$$K_{\text{H}_2\text{O}} = \frac{g}{\nu} \frac{1}{C_{KC}} \frac{1}{S_0^2} \frac{n^3}{(1 - n)^2}, \quad (23)$$

324 where  $S_0$  is the specific surface of particles, equal to  $S_0 = 6/d$  for uniform spheres and  
 325  $C_{KC} = 4.8$ . Moreover, the approach by [50] suggests that:

$$K_{\text{H}_2\text{O}} = 5.39 \cdot 10^4 \frac{D^2 e^3}{(1 + e)}, \quad (24)$$

326 where  $D$  is the diameter of the particles,  $e$  is the void ratio. Equation (24) refers to  
 327 porous media consisting of homogeneous spheres with a single diameter  $D$ . The values  
 328 of  $K_{\text{H}_2\text{O}}$  for the stratified specimens can be calculated as the harmonic mean of the  
 329 water permeabilities of the three homogeneous layers of equal thickness  $h_i = 2$  cm, for  
 330  $i = 1, 2, 3$ :

$$K_{\text{H}_2\text{O}} = \frac{\sum_{i=1}^3 h_i}{\sum_{i=1}^3 \frac{h_i}{K_{\text{H}_2\text{O},i}}} = 1.25 \cdot 10^{-3} \text{ m s}^{-1}. \quad (25)$$

331 All the empirical relationships return the hydraulic conductivity of a porous medium  
 332 as a function of the porosity and of the viscosity of the fluid. We bare in mind that each



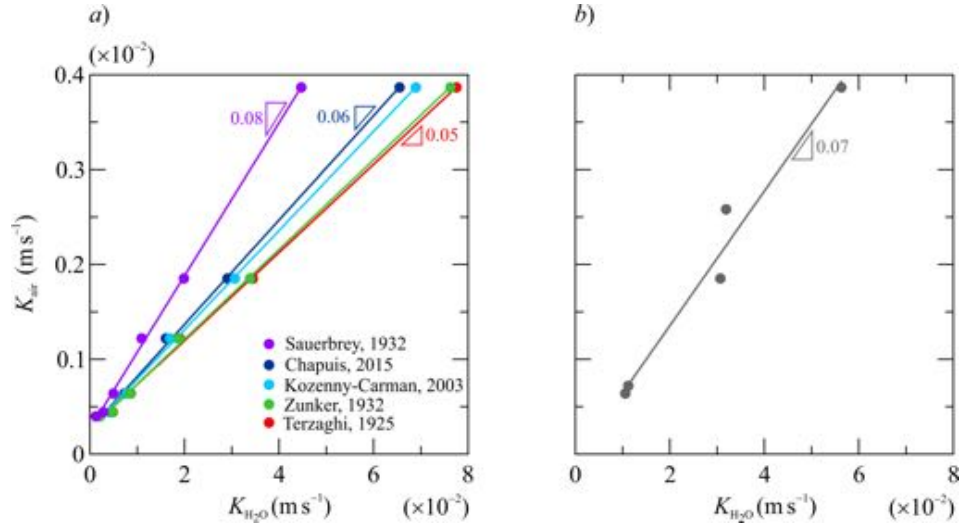


Figure 7: Experiments 1-7 with glass beads, 1-D permeameter. *a*) Measured air conductivity,  $K_{air}$ , plotted versus the hydraulic conductivity,  $K_{H_2O}$ , calculated through literature models for different kind of porous media; *b*) experimental air conductivity versus experimental water conductivity for specimens 3, 4, 5, 9, 10.

test #	$d$ (mm)	$K_{air} (\times 10^{-3}) (m s^{-1})$	$K_{H_2O} (\times 10^{-3}) (m s^{-1})$					Mean	Std
			Terzaghi (1925)	Sauebrej (1932)	Zunker (1932)	Kozeny-Carman (Carrier, 2003)	Chapuis (2015)		
1	0.5	0.40	1.82	1.24	2.12	1.92	1.82	1.77	0.29
2	0.75	0.44	4.09	2.79	4.77	4.31	4.09	3.89	0.72
3	1	0.64	7.28	4.96	8.47	7.66	7.28	6.80	1.42
4	2	1.85	29.11	19.86	33.89	30.64	29.11	26.30	7.17
5	3	3.87	65.49	44.68	76.25	68.95	65.49	58.26	17.90
6	1-2-3	1.22	16.04	10.94	18.67	16.89	16.04	14.79	3.43
7	3-2-1	1.16	16.04	10.94	18.67	16.89	16.04	14.79	3.43

Table 4: Comparison between the experimental air conductivity and the theoretical water conductivity. Porous medium of glass beads.

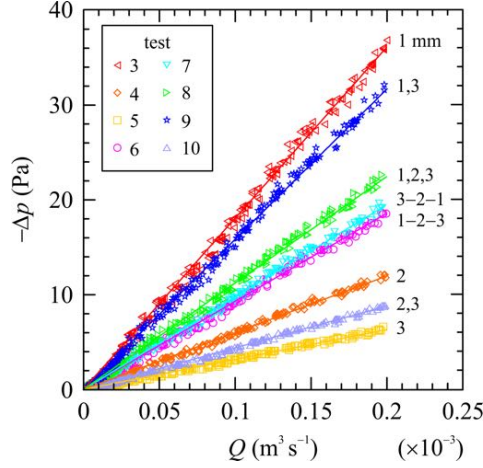


Figure 8: Glass beads specimens, differential pressure  $-\Delta p$  as a function of the air flow rate  $Q$  in a 1-D flow geometry. The legend indicates the number of the tests that symbols refer to.

333 study refers to a medium with different properties (natural or artificial medium, with  
 334 smooth or rough, rounded or irregular grains, etc.). This is the reason for the variability  
 335 of the results which are shown in figure 7a, where the measured air conductivity is plotted  
 336 versus the hydraulic conductivity calculated through literature models.

337 The numbers shown at the top of each straight line in figure 7a, represent the slope of  
 338 the empirical models, with values in the range  $0.05 - 0.13$ , so  $K_{\text{air}} = (0.05 - 0.13) K_{\text{H}_2\text{O}}$ ,  
 339 or alternatively  $K_{\text{H}_2\text{O}} = (7.7 - 20) K_{\text{air}}$ , which is consistent with eq. (15), derived from  
 340 dimensional analysis. Figure 7b shows the correlation between experimental air and  
 341 water conductivity for some specimens of the present study. The slope 0.07 of the line  
 342 lies in the theoretical range, and suggests that  $r_K = 1/0.07 \approx 15$ . This value of the  
 343 scaling factor can be adopted to estimate the water conductivity of a porous medium  
 344 (made of coarse glass beads) from the measured air conductivity.

345 Figure 8 shows the raw data of the differential pressure,  $-\Delta p$ , as a function of the flow  
 346 rate,  $Q$  for the experiments 1 – 10. The flow resistance increases for decreasing diameter  
 347 as expected, with the mixtures and the stratified specimens presenting an intermediate  
 348 response compared to their single components.

349 We can observe that:

- 350 • in the homogeneous samples, the conductivity increases with increasing glass beads  
 351 diameter. As expected, with the growth of the particle dimension, also the void  
 352 volume grows and the medium become more pervious;
- 353 • the difference in the conductivity of the stratified specimens (1–2–3 and 3–2–1)  
 354 is not significant, even though the conductivity in the fine-coarse direction,  $K_{\text{air}} =$   
 355  $1.22 \cdot 10^{-3} \text{ m s}^{-1}$ , is 5% greater than in the coarse-fine direction,  $K_{\text{air}} = 1.16 \cdot$   
 356  $10^{-3} \text{ m s}^{-1}$ , although the difference is well within the uncertainties. This was also  
 357 found by [51] who associated this difference to an abrupt drop of the pressure at the  
 358 interface between two media with different conductivity. This pressure drop induces  
 359 an extra energy loss and reduced the overall conductivity of the stratified medium.

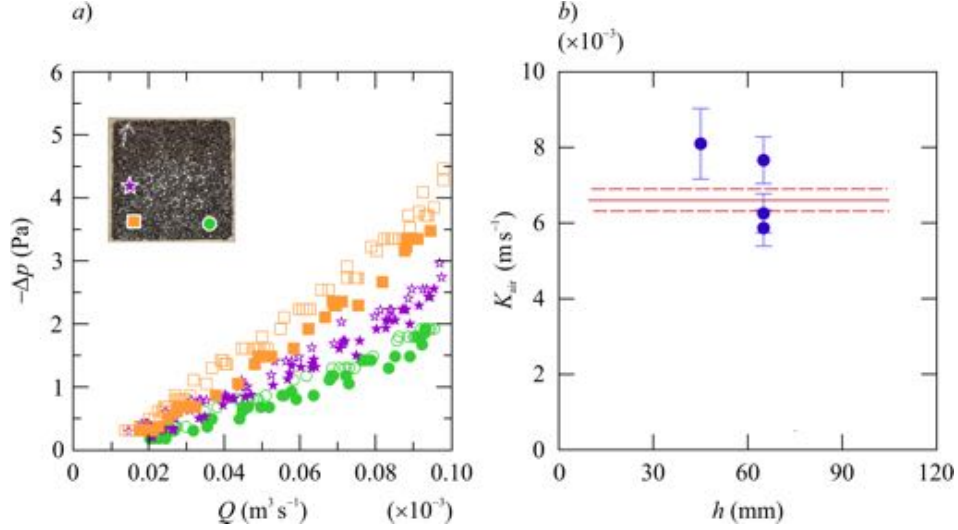


Figure 9: Asphalt samples, measurements on cores extracted from plates, 1-D flow configuration. *a*) Differential pressure  $-\Delta p$  as a function of the air flow rate  $Q$  for cores from the same plate with thickness  $h = 65$  mm; *b*) air conductivity  $K_{\text{air}}$  as a function of the thickness of the asphalt plate  $h$ . The solid red line represents the weighted average value, while the dotted red lines represent one weighted standard deviation.

360 However, we notice that this result is odd, since we expect larger dissipation, with  
 361 a consequent reduced conductivity, for the expansion process of the flow in the  
 362 fine-coarse direction;

- 363 • the value of the conductivity of the 2, 3 mixed specimen approximates the average of  
 364 the conductivity of the single components. This is a consequence of an intermediate  
 365 distribution of the voids between the 3 mm and 2 mm particles;
- 366 • the value of the conductivity of the 1, 3 mixed specimen is a little greater than the  
 367 conductivity of the homogeneous specimen with 1 mm beads. A possible explanation  
 368 is the greater difference between the 1 mm and 3 mm particles than the 2 mm  
 369 and 3 mm particles. The empty spaces between the beads is more efficiently filled  
 370 by the smallest particles, resulting in a slightly permeable medium.

### 371 5.2. 1-D hydraulic conductivity of asphalt samples

372 If we consider a heavy rainfall with intensity of  $100 \text{ mm h}^{-1}$ , and a circular cross-  
 373 section with diameter of 100 mm, the water flux entering the sample results  $Q_{\text{H}_2\text{O},r} =$   
 374  $0.22 \cdot 10^{-6} \text{ m}^3 \text{ s}^{-1}$ . The equivalent air flow rate is 10 times bigger, according to the  
 375 dimensional analysis described in § 2, so  $Q_{\text{air},r} = 0.22 \cdot 10^{-5} \text{ m}^3 \text{ s}^{-1}$ . We remind you that  
 376 the flow rate mainly depends on the flow of the adjacent pavement area, which can be  
 377 much higher than the local influx, especially at the borders of the road.

378 The differential pressure  $-\Delta p$  for the vertical conductivity of the cylindrical samples,  
 379 shows a linear trend with the air flow rate  $Q$ , for  $Q \leq 0.10 \cdot 10^{-3} \text{ m}^3 \text{ s}^{-1}$ , as it can be  
 380 seen in figure 9a. This value is two order of magnitude greater than  $Q_{\text{air},r}$ . This suggests

381 that, even during a rainfall such as the one described above, the flow through the asphalt  
 382 pores of the pavement is laminar.

383 Figure 9a refers to three samples cored from the asphalt plate with thickness  $h =$   
 384  $65$  mm. In the inset, the same symbols of the plots were used to indicate the region of  
 385 the asphalt plate where the samples had been cored from. The measurements show some  
 386 hysteresis, as the increasing (empty symbols) and decreasing (full symbols) branches do  
 387 not superpose perfectly. In addition, the slope of straight fitting lines varies. This could  
 388 be due to some damage caused by coring operations on small samples, since no hysteresis  
 389 can be seen on the original asphalt plates, as discussed later, in § 5.3.

390 Figure 9b shows the valued of the air conductivity of the three samples cored from  
 391 the plate with thickness  $h = 65$  mm and the value of one samples cored from the plate  
 392 with thickness  $h = 45$  mm.

393 The mean value for the air conductivity is evaluated as a weighted average,  $\bar{K}_{\text{air}}$ ,  
 394 with a weighted standard deviation,  $\sigma_K$ , which are shown as a solid line and two dotted  
 395 lines respectively in figure 9b, and calculated as follows:

$$\bar{K}_{\text{air}} = \frac{\sum \frac{1}{\sigma_i^2} K_{\text{air},i}}{\sum \frac{1}{\sigma_i^2}} = 6.6 \cdot 10^{-3} \text{ m s}^{-1}, \quad (26)$$

$$\sigma_K = \sqrt{\frac{1}{\sum \frac{1}{\sigma_i^2}}} = 0.3 \cdot 10^{-3} \text{ m s}^{-1}. \quad (27)$$

396 The extrapolated water conductivity is then  $K_{\text{H}_2\text{O}} \approx 10K_{\text{air}} \equiv (6.6 \pm 0.3) \cdot 10^{-2} \text{ m s}^{-1}$ .

### 397 5.3. Tests on the asphalt plates

398 Figure 10a shows the differential pressure,  $-\Delta p$ , against the air flow rate,  $Q$ , measured  
 399 by the field air permeameter, for five plates with increasing thickness. These data were  
 400 collected prior to the drilling operations. In spite of the plate with  $h = 65$  mm, the  
 401 flow resistance increases for decreasing thickness, since the influence of the impervious  
 402 condition at bottom of the plate may become relevant on the three dimensional structure  
 403 of the flow.

404 Figure 10b shows the linear relationship between the pressure and the air flow rate  
 405 for all the measuring points of the plates with different thickness, in the limit  $Q <$   
 406  $0.20 \cdot 10^{-3} \text{ m}^3 \text{ s}^{-1}$ .

407 The straight lines in figure 10a fit the data recorded for all the nine points of mea-  
 408 surements for each asphalt plate, and the correlation coefficient is always greater then  
 409 0.95. We also evaluated the parameter  $a$  separately for each measurement point of the  
 410 same plate, but there is not significant difference from the mean value. This indicates  
 411 that there are not preferential flow paths due to the roll compaction of the sample, and  
 412 the conductivity of the plate is uniform in space.

### 413 5.4. Evaluation of an equivalent dimensionless length scale for asphalt plates

414 In the case of the asphalt plates, we suggest that the main part of the flow can be  
 415 described as the radial flow across an annulus with inner radius  $r_1$ , outer radius  $r_2$ , and

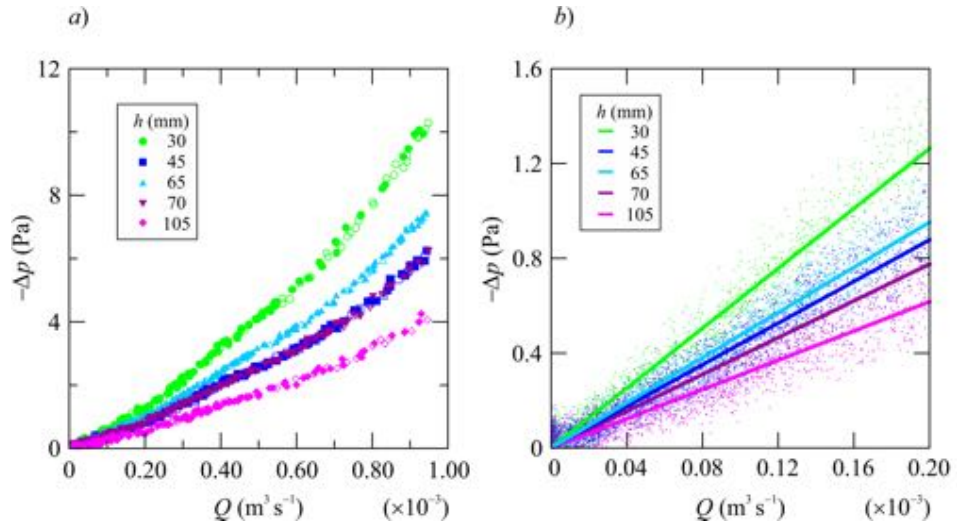


Figure 10: Asphalt plates, radial flux geometry. Differential pressure-discharge measurements for plates with different thickness. The measurements refer to the PMMA pipe positioned at the centre of the plate (point 5). (a) Whole set of data; (b) Data in the limit  $Q < 0.20 \cdot 10^{-3} \text{ m}^3 \text{ s}^{-1}$ .

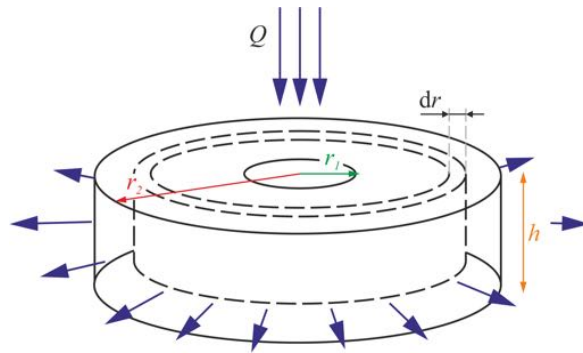


Figure 11: Schematic for the definition of the equivalent non dimensional length scale.

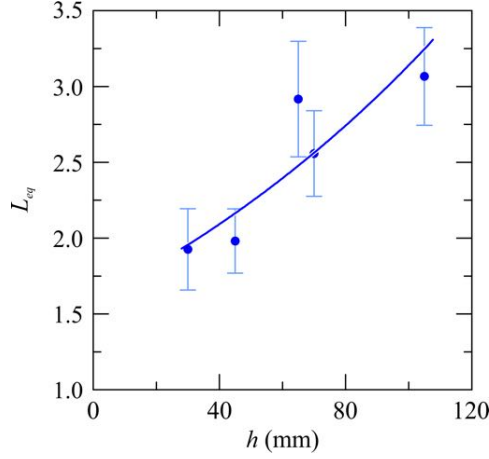


Figure 12: Equivalent non dimensional length scale  $L_{eq}$  as a function of the thickness  $h$  of the asphalt plates. Error bars are  $\pm 1$  standard deviation.

416 thickness  $h$ , as shown in figure [11](#). The Darcy formula for the annulus of thickness  $dr$  is

$$dQ = \frac{K_{\text{air}} 2\pi r h}{\gamma_{\text{air}}} \frac{dp}{dr}, \quad (28)$$

417 where  $2\pi r h$  is the lateral area of a cylinder with radius  $r$ , and  $dp/dr$  is the pressure  
418 gradient. We can integrate eq. [\(28\)](#) by separation of the variables, obtaining:

$$L_{eq} \equiv \frac{r_2}{r_1} = \exp\left(\frac{K_{\text{air}} 2\pi h a}{\gamma_{\text{air}}}\right). \quad (29)$$

419 The ratio  $L_{eq} = r_2/r_1$  is an equivalent non dimensional length scale relative to the  
420 asphalt plates. It can be evaluated as a function of the mean value of 1-D conductivity  
421  $K_{\text{air}}$  measured on the cylindrical samples (eq. [26](#)), on the thickness  $h$  and parameter  $a$   
422 of the asphalt plate. Figure [12](#) shows the experimental  $L_{eq}$  as a function of  $h$ , for all the  
423 asphalt plates.

424 All the experimental data are consistent with the theoretical model within one stan-  
425 dard deviation, with the exception of the asphalt plate with thickness  $h = 65$  mm.  
426 The experimental equation that allows the computation of  $L_{eq}$  on the basis of the only  
427 thickness  $h$ , is:

$$L_{eq} = 1.6 \exp(0.007 h) \approx 1.6 + 0.11 h, \quad \text{for } 30 < h < 110 \text{ mm}, \quad (30)$$

428 with  $h$  expressed in mm ( $R^2 = 0.80$ ). Inverting eq. [\(29\)](#) yields

$$K_{\text{air}} \approx \frac{\gamma_{\text{air}}}{2\pi h a} \ln(1.6 + 0.11h), \quad \text{for } 30 < h < 110 \text{ mm}. \quad (31)$$

### 429 5.5. In situ experiments

430 A series of field tests were conducted to compare the value of  $r_K$  predicted by dimen-  
431 sional analysis (eq. [15](#)) with field data. The available sites were (i) a service road inside

432 the Monza (Milan, Italy) racetrack and (ii) a urban road under construction in Poviglio  
 433 (Reggio Emilia, Italy). The thickness of the porous asphalt pavement in Monza is  $h = 70$   
 434 mm, while in Poviglio it is  $h = 40$  mm. The parameters of the field tests are listed in  
 435 tables [2](#)–[3](#).

436 Firstly, in both sites, we positioned the air field permeameter on the road axis, in  
 437 the middle of the lanes, and close to the edges, at different cross-sections of the roads,  
 438 and we measured the  $a$  parameter. The equivalent non dimensional length scale  $L_{eq}$   
 439 was estimated according to eq. [\(30\)](#) and the results show that  $L_{eq} = 0.94$  in Monza and  
 440  $L_{eq} = 0.74$  in Poviglio. The air conductivity can be estimated by reversing eq. [\(29\)](#):

$$K_{\text{air}} = \frac{\gamma_{\text{air}}}{2\pi ha} \ln(L_{eq}) \quad (32)$$

441 The mean values for the air conductivity are  $K_{\text{air}} = (0.43 \pm 0.02) \cdot 10^{-3} \text{ m s}^{-1}$  in Monza  
 442 and  $K_{\text{air}} = (1.00 \pm 0.08) \cdot 10^{-3} \text{ m s}^{-1}$  in Poviglio.

443 Secondly, we measured the water conductivity by the falling head permeameter in  
 444 some of the points where the  $K_{\text{air}}$  value was available. The mean values are  $K_{\text{H}_2\text{O}} =$   
 445  $(4.1 \pm 0.5) \cdot 10^{-3} \text{ m s}^{-1}$  in Monza and  $K_{\text{H}_2\text{O}} = (5.1 \pm 0.8) \cdot 10^{-3} \text{ m s}^{-1}$  in Poviglio.

446 As a consequence the scale factors for the conductivity is  $r_K = 9.6$  in Monza and  
 447  $r_K = 5.1$  in Poviglio, which are of the same order of magnitude as predicted by the  
 448 dimensional analysis,  $r_K = \mathcal{O}(10)$ .

449 We now shall compare our results with previous studies found in literature. Figure [13](#)  
 450 gives an overview of the range of the hydraulic conductivity values of porous asphalt  
 451 pavements, measured using falling head permeameters. The results by different authors  
 452 are of the same order of magnitude and the differences can be addressed (i) to the  
 453 different mix design of the asphalt mixtures and (ii) to the specific characteristics of the  
 454 permeameter used by the authors.

455 As mentioned in § [1](#), [16](#) used two methods to test the water conductivity of porous  
 456 asphalt pavements, the National Center for Asphalt Technology (NCAT) falling head per-  
 457 meameter and ASTM C1701 constant head permeameter. They found that the conduc-  
 458 tivity measured with the ASTM method lies in the range  $K_{\text{H}_2\text{O}} = (0.6 - 1.1) \cdot 10^{-3} \text{ m s}^{-1}$   
 459 and are 70% on average lower than the value measured with the NCAT method, which  
 460 falls in the range  $K_{\text{H}_2\text{O}} = (9.4 - 12) \cdot 10^{-3} \text{ m s}^{-1}$ .

461 On the other hand, [52](#) used the Laboratorio de Caminos de Santander (LCS) per-  
 462 meameter to measure the horizontal and vertical hydraulic conductivity on field plates  
 463 as a function of the voids content. For voids content between 21 – 29% the vertical  
 464 conductivity grows from 3.2 to  $9 \cdot 10^{-3} \text{ m s}^{-1}$ .

465 Lu *et al.* (2020) [53](#) investigated the conductivity of polyurethane-bound pervious  
 466 materials, with effective porosity of approximately 28 – 29%, using a custom-made con-  
 467 stant head permeameter developed according to the UNI EN 12697/19 protocol. They  
 468 found that  $K_{\text{H}_2\text{O}} = (3.4 - 5.3) \cdot 10^{-3} \text{ m s}^{-1}$ .

469 Each method has its advantages and disadvantages. This is principally why there  
 470 are a lot of techniques and types of permeameters used by different authors in previous  
 471 studies. For example, [16](#) discuss the implications of the results obtained by using the  
 472 ASTM C1701 and NCAT permeameters. They say that the size of the permeameter ring  
 473 may affect the results, as well as whether the measurements are made under constant  
 474 head or falling head conditions. As it happens, ASTM C1701 gives higher values of  
 475 permeability if operating under falling head than under constant head. Moreover, NCAT

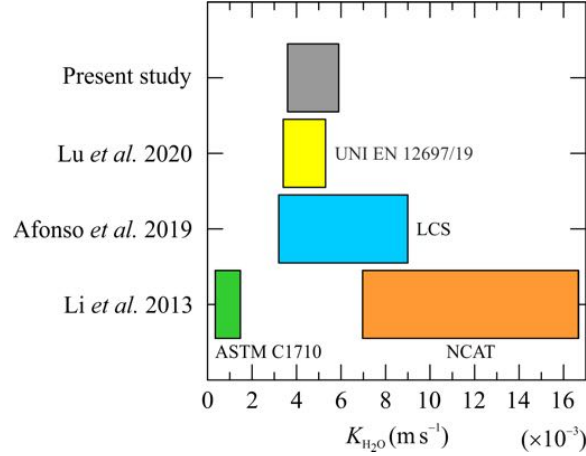


Figure 13: Comparison of values of the water conductivity  $K_{H_2O}$  from literature and present experiments.

476 method is more affected by errors in the knowledge of the thickness of the pavement than  
 477 the ASTM, but at the same time, NCAT is based on a better established falling head  
 478 theory derived by the Darcy's law, while the equation used in the ASTM method are not  
 479 well explained. Similarly, [52] state that the results obtained with EN 12697-40 and EN  
 480 12697-19 are not directly comparable to each other and to other methods as well, such  
 481 as the LCS.

482 Different ranges of the measured conductivity may arise because of misunderstanding  
 483 of definitions and using of non-standard terminology between different authors, such as  
 484 saturated hydraulic conductivity [20], infiltration capacity [6], permeability coefficient  
 485 [54], or simply permeability [55, 24].

## 486 6. Conclusion

487 This paper presented a novel apparatus for measuring the in situ conductivity of  
 488 porous asphalt pavements. This apparatus consists of a simple PMMA tube as air  
 489 permeameter, a mass flow meter, a pressure gauge and a laptop for calibration and data  
 490 acquisition. The positive sides of using air as fluid are that (i) a little time is necessary  
 491 to establish pressure flow equilibrium, (ii) there is no need to carry a huge amount of  
 492 fluid on site, as air is immediately available everywhere, (iii) the nature of the test is non  
 493 destructive, as the crack size is not altered by the air flow, if applied for a short time.

494 The main conclusion are the followings.

- 495 • The 1-D permeameter was firstly calibrated using glass beads specimens. The  
 496 ratio between the measured air and water conductivity is  $r_K = 7.7$ . This value is  
 497 consistent with the value  $r_K \approx 10$  suggested by dimensional analysis.
- 498 • Secondly, the air field permeameter was used in laboratory to estimate the pa-  
 499 rameter  $a = -\Delta p/Q$  of asphalt plates with variable thickness. The vertical air  
 500 conductivity of the asphalt plates was measured separately, using the Darcy for-  
 501 mula, on cylindrical samples cored from each plate.



- 502 • We then derived a simple model for an estimate of an equivalent non dimensional  
503 length scale,  $L_{eq}$ , based on the knowledge of the only thickness of the porous asphalt  
504 plate. The value of  $L_{eq}$  could be used on site, together with the  $a$  parameter given  
505 by the air field permeameter, in order to compute the conductivity of the asphalt  
506 layer.
- 507 • Finally, some field tests were conducted on two available sites, in order to estimate  
508 the scale ratio  $r_K$  in field. The results are  $r_K = 9.6$  in Monza and  $r_K = 5.1$  in  
509 Poviglio, which are of the same order of magnitude as predicted by the dimensional  
510 analysis ( $r_K = 10$ ).

511 We remind the readers that a variability of the results is expected, since the dimen-  
512 sional analysis followed by experiments captures the relevant dimensional groups that  
513 control the process, but cannot describe in detail the relationship between these groups.  
514 In particular the relationship  $r_K$  is site-specific and allows to control the time variation  
515 of the same pavement due, for example, to clogging phenomena and to plan mainte-  
516 nance. The instrument and methodology can be easily used to measure the effects of  
517 porous asphalt pavement drainage control systems in order to limit the disposal of de-  
518 and anti-icing solutions.

519 Future studies may focus on the changing of hydraulic permeability, and so the  $r_K$   
520 parameter, because of crack propagation due to water damage or clogging phenomena.  
521 In this way the changing in  $r_K$  could be better related to a changing in the geometry  
522 of air voids. Also the effects of anisotropy of asphalt mixtures may be included in the  
523 theoretical model and measurement procedures, and the effects of surface tensions when  
524 water becomes in contact with pore edges.

## 525 Acknowledgements

526 This work was supported by the University of Parma - FIL incentivante 2019 - project:  
527 “Increased road safety on draining pavements through the development of percolation  
528 retardant fluids for anti-icing solutions.”

## 529 List of symbols and acronyms

$A$	cross-section area of the pipe, $L^2$
$A'$	cross-section area of the sample, $L^2$
$a$	slope of the straight line fitting the experimental data $-\Delta p$ versus $Q$ , $ML^{-4}T^{-1}$
ASTM	American Society for Testing and Materials
$b$	Klinkenberg slip coefficient, $ML^{-1}T^{-2}$
$c$	coefficient, (.)
$C_{KC,S,T,Z}$	constants, (.)
$D$	diameter, $L$
$D_{int}$	internal diameter, $L$
$e$	void ratio, (.)
Fr	Froude number, (.)
$g$	acceleration due to gravity, $LT^{-2}$

$H$	total head, $L$
$h$	thickness of asphalt plate, $L$
$J$	energy dissipation rate, $(.)$
$K$	conductivity, $LT^{-1}$
$K_{\text{air}}$	air conductivity, $LT^{-1}$
$K_{\text{H}_2\text{O}}$	water conductivity, $LT^{-1}$
$\text{Kn}$	Knudsen number, $(.)$
$k$	intrinsic permeability, $L^2$
$k_{\infty}$	asymptotic intrinsic permeability, $L^2$
$L$	characteristic length path, $L$
$l_1$	initial level in the falling head permeameter, $L$
$l_2$	final level in the falling head permeameter, $L$
$L_{eq}$	equivalent length scale, $L$
$l_m$	mean free path of molecules, $L$
LCS	Laboratorio Caminos Santander permeameter
LPC	Leeds Permeability Cell
$n$	porosity, $(.)$
NCAT	National Center for Asphalt Technology falling head permeameter
$p$	pressure, $ML^{-1}T^{-2}$
$Q$	flow rate, $L^3T^{-1}$
$r$	radial coordinate, $L$
$r_i$	scale ratio for the quantity $i$ , $(.)$
$r_1$	inner radius of the annulus, $L$
$r_2$	outer radius of the annulus, $L$
Re	Reynolds number, $(.)$
$S_0$	specific surface of particles, $L^{-1}$
$u$	velocity $LT^{-1}$
$\gamma_{\text{air}}$	air specific weight, $ML^{-2}T^{-2}$
$\gamma_{\text{H}_2\text{O}}$	water specific weight, $ML^{-2}T^{-2}$
$\Delta H$	head variation, $L$
$\Delta p$	differential pressure, $ML^{-1}T^{-2}$
$\Delta t$	time interval for the water column to flow through the sample, $T$
$\theta$	temperature, $\Theta$
$\kappa$	Boltzmann's constant, $ML^2T^{-2}\Theta^{-1}$
$\lambda$	length scale, $L$
$\mu$	dynamic viscosity, $ML^{-1}T^{-1}$
$\nu_{\text{air}}$	air kinematic viscosity, $L^2T^{-1}$
$\nu_{\text{H}_2\text{O}}$	water kinematic viscosity, $L^2T^{-1}$
$\rho$	density, $ML^{-3}$
$\sigma_K$	standard deviation of $K$ , $LT^{-1}$
$\Phi$	function

530 **References**

- 531 [1] G. Stotz, K. Krauth, The pollution of effluents from pervious pavements of an experimental highway  
532 section: first results, Science of the total environment 146 (1994) 465–70.

- 533 [2] C. Pagotto, M. Legret, P. Le Cloirec, Comparison of the hydraulic behaviour and the quality of  
534 highway runoff water according to the type of pavement, *Water Research* 34 (2000) 4446–54.
- 535 [3] J. Sansalone, X. Kuang, V. Ranieri, Permeable pavement as a hydraulic and filtration interface for  
536 urban drainage, *Journal of irrigation and drainage engineering* 134 (2008) 666–74.
- 537 [4] H. Imran, S. Akib, M. R. Karim, Permeable pavement and stormwater management systems: a  
538 review, *Environmental technology* 34 (2013) 2649–56.
- 539 [5] N. R. Siriwardene, A. Deletic, T. Fletcher, Clogging of stormwater gravel infiltration systems and  
540 filters: Insights from a laboratory study, *Water research* 41 (2007) 1433–40.
- 541 [6] V. C. Andres-Valeri, L. Juli-Gandara, D. Jato-Espino, J. Rodriguez-Hernandez, Characterization  
542 of the infiltration capacity of porous concrete pavements with low constant head permeability tests,  
543 *Water* 10 (2018) 480.
- 544 [7] Y. Ma, X. Chen, Y. Geng, X. Zhang, Effect of clogging on the permeability of porous asphalt  
545 pavement, *Advances in Materials Science and Engineering* 2020 (2020).
- 546 [8] M. Z. H. Mahmud, N. A. Hassan, M. R. Hainin, C. R. Ismail, R. P. Jaya, M. N. M. Warid, H. Yaacob,  
547 N. Mashros, Characterisation of microstructural and sound absorption properties of porous asphalt  
548 subjected to progressive clogging, *Construction and Building Materials* 283 (2021) 122654.
- 549 [9] D. M. Ramakrishna, T. Viraraghavan, Environmental impact of chemical deicers—a review, *Water,  
550 Air, and Soil Pollution* 166 (2005) 49–63.
- 551 [10] M. A. Cunningham, E. Snyder, D. Yonkin, M. Ross, T. Elsen, Accumulation of deicing salts in  
552 soils in an urban environment, *Urban Ecosystems* 11 (2008) 17–31.
- 553 [11] X. Shi, D. Veneziano, N. Xie, J. Gong, Use of chloride-based ice control products for sustainable  
554 winter maintenance: A balanced perspective, *Cold Regions Science and Technology* 86 (2013)  
555 104–12.
- 556 [12] F. Autelitano, M. Rinaldi, F. Giuliani, Winter highway maintenance strategies: Are all the sodium  
557 chloride salts the same?, *Construction and Building Materials* 226 (2019) 945–52.
- 558 [13] UNI, Bituminous mixtures - Test methods for hot mix asphalt - Part 40: In situ drainability,  
559 Technical Report EN 12697-40:2006, 2006.
- 560 [14] ASTM International, Standard Test Method for Infiltration Rate of In Place Pervious Concrete,  
561 Technical Report ASTM Designation: C1701 / C1701M-09, 2009.
- 562 [15] ASTM International, Standard Test Method for Surface Infiltration Rate of Permeable Unit Pave-  
563 ment Systems, Technical Report ASTM Designation: C1781 / C1781M-18e1, 2018.
- 564 [16] H. Li, M. Kayhanian, J. T. Harvey, Comparative field permeability measurement of permeable  
565 pavements using ASTM C1701 and NCAT permeameter methods, *Journal of Environmental Man-  
566 agement* 118 (2013) 144–52.
- 567 [17] L.-M. Chen, J.-W. Chen, T.-H. Chen, T. Lecher, P. C. Davidson, Measurement of permeability  
568 and comparison of pavements, *Water* 11 (2019) 444.
- 569 [18] MTC, Permeabilidad in situ de pavimentos drenantes con el permeámetro LCS, Technical Report  
570 NLT 327/00, Ministerio de Transportes y Comunicaciones, 2000.
- 571 [19] M. T. Van Genuchten, A closed-form equation for predicting the hydraulic conductivity of unsat-  
572 urated soils, *Soil Science Society of America Journal* 44 (1980) 892–8.
- 573 [20] P. Blackwell, A. Ringrose-Voase, N. Jayawardane, K. Olsson, D. McKenzie, W. Mason, The use of  
574 air-filled porosity and intrinsic permeability to air to characterize structure of macropore space and  
575 saturated hydraulic conductivity of clay soils, *Journal of Soil Science* 41 (1990) 215–28.
- 576 [21] B. V. Iversen, P. Moldrup, P. Schjønning, O. H. Jacobsen, Field application of a portable air  
577 permeameter to characterize spatial variability in air and water permeability, *Vadose Zone Journal*  
578 2 (2003) 618–26.
- 579 [22] H. Li, J. J. Jiao, M. Luk, A falling-pressure method for measuring air permeability of asphalt in  
580 laboratory, *Journal of Hydrology* 286 (2004) 69–77.
- 581 [23] D. S. Springer, H. A. Loaiciga, S. J. Cullen, L. G. Everett, Air permeability of porous materials  
582 under controlled laboratory conditions, *Ground Water* 36 (1998) 558–65.
- 583 [24] T. Wells, S. Fityus, D. W. Smith, Use of in situ air flow measurements to study permeability in  
584 cracked clay soils, *Journal of Geotechnical and Geoenvironmental Engineering* 133 (2007) 1577–86.
- 585 [25] J. Cabrera, C. Lynsdale, A new gas permeameter for measuring the permeability of mortar and  
586 concrete, *Magazine of Concrete Research* 40 (1988) 177–82.
- 587 [26] J. Cabrera, T. Hassan, Quality control during construction of bituminous mixtures using a simple  
588 air permeability test, in: *Performance and Durability of Bituminous Materials*, Proceedings of  
589 Symposium, University of Leeds, 1996.
- 590 [27] S. E. Zoorob, J. G. Cabrera, L. B. Suparma, A gas permeability method for controlling quality  
591 of dense bituminous composites, *Proc. 3rd European Symposium: Performance and Durability of*

- 592 Bituminous Materials and Hydraulic Stabilised Composites (1999) 549–72.
- 593 [28] D. L. Allen, D. B. Schultz Jr, L. J. Fleckenstein, Development and proposed implementation of a  
594 field permeability test for asphalt concrete, Technical Report KTC-01-19/SPR216-001F, University  
595 of Kentucky, 2001.
- 596 [29] D. Perraton, A. Carter, In-situ permeability of the outermost layer of asphalt and cement concrete  
597 road materials: Water permeability evaluated with gas flow, *Road Materials and Pavement Design*  
598 6 (2005) 239–53.
- 599 [30] P. Vardanega, State of the art: Permeability of asphalt concrete, *Journal of Materials in Civil*  
600 *Engineering* 26 (2012) 54–64.
- 601 [31] J. Chen, H. Wang, H. Zhu, Investigation of permeability of open graded asphalt mixture considering  
602 effects of anisotropy and two-dimensional flow, *Construction and Building Materials* 145 (2017)  
603 318–25.
- 604 [32] E. Masad, A. Al Omari, H.-C. Chen, Computations of permeability tensor coefficients and  
605 anisotropy of asphalt concrete based on microstructure simulation of fluid flow, *Computational*  
606 *Materials Science* 40 (2007) 449–59.
- 607 [33] I. Gruber, I. Zinovik, L. Holzer, A. Flisch, L. D. Poulikakos, A computational study of the effect  
608 of structural anisotropy of porous asphalt on hydraulic conductivity, *Construction and Building*  
609 *Materials* 36 (2012) 66–77.
- 610 [34] V. Di Federico, R. Archetti, S. Longo, Similarity solutions for spreading of a two-dimensional  
611 non-Newtonian gravity current in a porous layer, *Journal of Non-Newtonian Fluid Mechanics* 177  
612 (2012) 46–53.
- 613 [35] V. Di Federico, R. Archetti, S. Longo, Spreading of axisymmetric non-Newtonian power-law gravity  
614 currents in porous media, *Journal of Non-Newtonian Fluid Mechanics* 189 (2012) 31–9.
- 615 [36] V. Di Federico, S. Longo, S. King, L. Chiapponi, D. Petrolo, V. Ciriello, Gravity-driven flow of  
616 Herschel–Bulkley fluid in a fracture and in a 2D porous medium, *Journal of Fluid Mechanics* 821  
617 (2017) 59–84.
- 618 [37] L. Chiapponi, V. Ciriello, S. Longo, V. Di Federico, Non-Newtonian backflow in an elastic fracture,  
619 *Water Resources Research* 55 (2019) 10144–58.
- 620 [38] B. S. Massey, Units, dimensional analysis and physical similarity, Van Nostrand Reinhold, 1971.
- 621 [39] S. Longo, *Analisi Dimensionale e Modellistica Fisica: Principi e Applicazioni alle Scienze Ingegner-*  
622 *istiche (Dimensional Analysis and Physical Modeling: Principles and Applications in Engineering)*  
623 (in italian), Springer Science & Business Media, 2011.
- 624 [40] L. Klinkenberg, The permeability of porous media to liquids and gases, in: *Drilling and production*  
625 *practice*, American Petroleum Institute, 1941.
- 626 [41] D. Faulkner, E. Rutter, Comparisons of water and argon permeability in natural clay-bearing fault  
627 gouge under high pressure at 20 °C, *Journal of Geophysical Research: Solid Earth* 105 (2000)  
628 16415–26.
- 629 [42] Y.-S. Wu, K. Pruess, P. Persoff, Gas flow in porous media with Klinkenberg effects, *Transport in*  
630 *Porous Media* 32 (1998) 117–37.
- 631 [43] L. A. Cooley Jr, Permeability of Superpave mixtures: evaluation of field permeameters, Technical  
632 Report National Center for Asphalt Technology, NCAT Report, Auburn University, 1999.
- 633 [44] L. Chiapponi, Water retention curves of multicomponent mixtures of spherical particles, *Powder*  
634 *Technology* 320 (2017) 646–55.
- 635 [45] J. Říha, L. Petrula, M. Hala, Z. Alhasan, Assessment of empirical formulae for determining the  
636 hydraulic conductivity of glass beads, *Journal of Hydrology and Hydromechanics* 66 (2018) 337–47.
- 637 [46] K. Terzaghi, Principles of soil mechanics, *Engineering News-Record* 95 (1925) 19–32.
- 638 [47] F. Zunker, *Zeitschrift fur pflanzenenerwehung (Fertilization and Soil Science)*, *Duengung und Bo-*  
639 *denkunde (Journal for Plant Nutrition)* 25 (1932) 1.
- 640 [48] I. Sauerbrey, On the problem and determination of the permeability coefficient, *Proceedings VNIIG*  
641 (1932).
- 642 [49] W. D. Carrier III, Goodbye, Hazen; hello, Kozeny-Carman, *Journal of Geotechnical and Geoenvi-*  
643 *ronmental Engineering* 129 (2003) 1054–6.
- 644 [50] R. P. Chapuis, S. Weber, F. Duhaime, Permeability test results with packed spheres and non-plastic  
645 soils, *Geotechnical Testing Journal* 38 (2015) 950–64.
- 646 [51] Z. Li, D. Wang, X. Zhang, J. W. Crawford, Water flow across the interface of contrasting materials:  
647 Pressure discontinuity and its implications, *Journal of Hydrology* 566 (2018) 435–40.
- 648 [52] M. I. L. Afonso, T. S. Santos, C. M. S. Fael, M. S. D. Almeida, Hydraulic conductivity of the  
649 permeable asphalt pavement–laboratory vs in situ test, in: *IOP Conference Series: Materials*  
650 *Science and Engineering*, volume 471, 2019, p. 022023.

- 651 [53] G. Lu, Z. Wang, P. Liu, D. Wang, M. Oeser, Investigation of the hydraulic properties of pervious  
652 pavement mixtures: Characterization of darcy and non-darcy flow based on pore microstructures,  
653 *Journal of Transportation Engineering, Part B: Pavements* 146 (2020) 04020012.
- 654 [54] P. Bamforth, The relationship between permeability coefficients for concrete obtained using liquid  
655 and gas, *Magazine of concrete research* 39 (1987) 3–11.
- 656 [55] R. G. Shepherd, Correlations of permeability and grain size, *Groundwater* 27 (1989) 633–8.